Acta Cryst. (1988). B44, 108–116

Incommensurate Modulated Structure of $BaMnF_4$ with Monoclinic Symmetry at 100 and 210 K

BY PH. SCIAU AND J. LAPASSET

Groupe de dynamique des phases condensées, LA CNRS 233, Université des Sciences et Techniques du Languedoc, 34060 Montpellier CEDEX, France

AND D. GREBILLE† AND J. F. BERAR

Laboratoire de chimie-physique du solide, UA CNRS 453, Ecole Centrale des Arts et Manufactures, 92295 Châtenay-Malabry CEDEX, France

(*Received* 30 *March* 1987; *accepted* 2 *November* 1987)

Abstract

The incommensurate modulated structure of $BaMnF_4$ has been refined at 210 K and at 100 K using symmetry properties of the four-dimensional superspace groups. Two main assumptions have been made: orthorhombic symmetry ($U^{P2_1nb}_{1\,qq}$) and monoclinic symmetry ($U^{A2_111}_{1\,11}$). The symmetry of the X-ray diffraction pattern is better described with the monoclinic hypothesis assuming a twinning of the crystal. Refinement results have confirmed this analysis [$R_F = 4{\cdot}51\%$ for 4321 reflections at 100 K (monoclinic), $R_F = 5{\cdot}61\%$ for 3844 reflections at 210 K (monoclinic), $R_F = 8{\cdot}1\%$ for 2217 reflections at 210 K (orthorhombic)]. The modulation is coherent with a rigid-body rotation of the MnF_6 octahedra and a related rectilinear motion of the Ba ion. A comparison of the shape and amplitude of the modulation waves at both temperatures is discussed.

Introduction

The compound $BaMnF_4$ presents numerous interesting physical properties and has been the subject of experimental or theoretical studies (Saint-Grégoire, 1985; Cox, Shapiro, Cowley, Eibschütz & Guggenheim, 1979). It also presents interesting structural properties and, in particular, a structural transition at 250 K from a high-temperature (HT) phase to an incommensurate modulated phase which has already been widely investigated. The crystal structure of $BaMnF_4$ has been solved at room temperature (Keve, Abrahams & Bernstein, 1969): $a = 5{\cdot}9845$, $b = 15{\cdot}098$, $c = 4{\cdot}2216$ Å, space group $A2_1am$, $Z = 4$.

The HT to incommensurate phase transition can be observed on the X-ray diffraction pattern; it involves the appearance of extra satellite reflections located at the positions $(\pm\xi, \pm\frac{1}{2}, \pm\frac{1}{2})$ of the reciprocal lattice of the HT phase, with $\xi \sim 0{\cdot}39$. Studies (Cox, Shapiro, Nelmes, Ryan, Bleif, Cowley, Eibschütz & Guggenheim, 1983; Barthès-Régis, Almairac, Saint-Grégoire, Filippini, Steigenberger, Nouet & Gesland, 1983; Saint-Grégoire, 1985) have shown a very small variation of ξ from 4 to 250 K and all have pointed out the absence of lock-in temperature; this is unusual behaviour for such modulated compounds.

As far as structure is concerned, two symmetries have been proposed for this modulated phase:

– orthorhombic symmetry (i) with point group $2mm$ (C_{2v}). The crystal is monodomain and modulated by the eight vectors of the star of the wavevector $q^* = (\pm\xi, \pm 0{\cdot}5, \pm 0{\cdot}5)$.

– monoclinic symmetry with point group 2 (C_2). Here, two cases have been considered. In the first, (ii), we suppose that the modulation is characterized by the star of the two wavevectors $\mathbf{q}_1^* = (\xi, 0{\cdot}5, 0{\cdot}5)$ and $\mathbf{q}_2^* = (\xi, -0{\cdot}5, 0{\cdot}5)$, for example (Cox *et al.*, 1983); in the second, (iii), we suppose that the crystal is the juxtaposition of twin domains characterized by one of the preceding wavevectors (iii).

The monoclinic hypothesis is compatible with the existence of the magnetoelectric effect (Dvorak, 1975). The last one (iii) has recently been confirmed by two independent studies which have shown the splitting of some of the main reflections, the first by γ-ray diffraction (Saint-Grégoire, Almairac, Freund & Gesland, 1986) and the second by high-resolution X-ray diffraction (Ryan, 1986).

The first model for the incommensurate structure was proposed by Dvorak & Fousek (1980), and involves the rotation of the $Mn-F_6$ octahedra of the structure about the a axis.

In the present paper, we describe the symmetry properties of the incommensurate phase in the $(3 + d)$-dimensional formalism developed by de Wolff, Janssen & Janner (1981).

We have studied and refined this structure using the expression of the structure factor derived by Yamamoto (1982*a*). In a previous paper, we gave preliminary results using data recorded at 100 K containing only

† To whom correspondence should be addressed.

0108-7681/88/020108-09$03.00

first-order satellites and we restricted our analysis to the apparent orthorhombic symmetry (i) (Sciau, Grebille, Bérar & Lapasset, 1986). In the present paper, we show that a more complete analysis of the X-ray diffraction pattern (extinction rules of the second-order satellites) allows confirmation of the splitting of the crystal into two types of monoclinic twin domains [hypothesis (iii)]. It is then possible to determine the structure of one domain and the relative ratio of each domain in the whole crystal. This study has been carried out at two different temperatures (100 and 210 K).

Experimental

Intensity measurements were performed using a spherical crystal (radius 0·105 mm) provided by Dr Gabbe (MIT). They have been obtained on an Enraf–Nonius CAD-3 diffractometer (graphite-monochromated Mo $K\alpha$ radiation) at 100 and 210 K. The crystal was cooled by a stream of nitrogen gas (stability ± 2 K). At both temperatures, the crystal was kept at a stabilized temperature over the whole period of data collection to avoid hysteresis phenomena and fluctuations of the relative domain ratio during the phase transition (over 250 K). The crystal was brought to room temperature between data collections at 100 and 210 K.

The cell parameters are: $a = 6{\cdot}01$ (1), $b = 15{\cdot}16$ (3), $c = 4{\cdot}22$ (1) Å at 210 K and $a = 6{\cdot}01$, $b = 15{\cdot}13$ (3), $c = 4{\cdot}22$ (1) Å at 100 K (using 20 reflections with $13° < \theta < 40°$). The incommensurate component of the modulation has been assumed to be 0·395 (at 210 K) and 0·399 (at 100 K). 6118 and 5333 reflections were measured with $(\sin\theta)_{max}/\lambda = 0{\cdot}71$ Å^{-1}; $0 \le h \le 9$, $-22 \le k \le 22$, $0 \le l \le 6$, $-2 \le m \le 2$, using a θ–2θ scan technique (scan width: $1{\cdot}2° + 0{\cdot}25\ \mathrm{tg}\theta$). After averaging of equivalent reflections, 3844 (669 main reflections, 2476 first-order and 699 second-order satellites) and 4321 (657 main reflections, 2567 first-order and 1097 second-order satellites) with $I > 3\sigma(I)$ were retained respectively at 210 and 100 K. About 800 third-order satellites were also measured with $10° < \theta < 15°$, but there were too few with $I > 3\sigma(I)$ to be included in the data collection for refinement. Lorentz–polarization and absorption corrections were applied ($\mu = 15{\cdot}05$ mm^{-1}; Escande, 1971). Three standard reflections (one main reflection, and two first-order satellites which did not belong to the same domain) were measured every 40 reflections. No significant fluctuation of their intensity was observed.

X-ray diffraction pattern and symmetry

The diffraction pattern of the incommensurate phase is similar to that of the HT phase ($T > 250$ K) as far as the main reflections are concerned. However, one can also observe weaker satellite reflections located at ($\pm\xi$, $\pm\frac{1}{2}$, $\pm\frac{1}{2}$) from the Bragg reflections (Fig. 1). The variation of ξ as a function of temperature has been widely studied (Cox *et al.*, 1983; Barthès-Régis *et al.*, 1983); when cooling from 250 to 4 K, ξ increases continuously from about 0·390 to a value belonging in the range 0·392–0·399, according to the sample. The respective values of ξ at 100 and 210 K for our sample are 0·399 and 0·395.

All reflections can apparently be indexed by four integers:

$$S = h\mathbf{a}^* + k\mathbf{b}^* + l\mathbf{c}^* + m\mathbf{q}^*, \qquad (1)$$

with ($\mathbf{a}^*$, $\mathbf{b}^*$, $\mathbf{c}^*$) basic vectors of the HT reciprocal space and $\mathbf{q}^* = \xi\mathbf{a}^* + (\mathbf{b}^*/2) + (\mathbf{c}^*/2)$. Satellites can easily be observed up to the second order ($m = \pm 1, \pm 2$).

Let us first consider the case of an orthorhombic monodomain crystal (i).

If we try to associate each satellite reflection with a Bragg reflection of the HT structure, there are eight first-order satellites around each Bragg node (Fig. 1). Then, if we take into account the HT A centring, we have to introduce three independent modulation vectors, for example:

$$\mathbf{q}_1^* = \xi\mathbf{a}^* + (\mathbf{b}^*/2) + (\mathbf{c}^*/2)$$
$$\mathbf{q}_2^* = \xi\mathbf{a}^* + (\mathbf{b}^*/2) - (\mathbf{c}^*/2)$$
$$\mathbf{q}_3^* = \xi\mathbf{a}^* - (\mathbf{b}^*/2) + (\mathbf{c}^*/2)$$

and we can write a six-dimensional indexing relation:

$$\mathbf{S} = h\mathbf{a}^* + k\mathbf{b}^* + l\mathbf{c}^* + m_1\mathbf{q}_1^* + m_2\mathbf{q}_2^* + m_3\mathbf{q}_3^* \qquad (2)$$

with the centring extinction rule:

$$h, k, l, m_1, m_2, m_3: k + l = 2n$$

In this case, there is no reason to constrain the y and z components of the wavevector $\mathbf{q}^*$ to $\frac{1}{2}$. As no variation

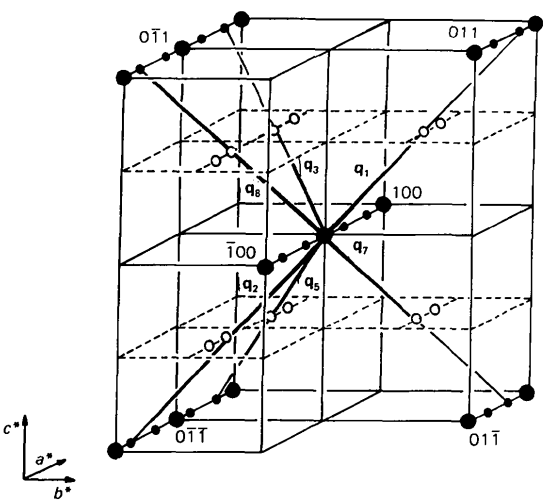

Fig. 1. Diffraction pattern of the incommensurate phase of $BaMnF_4$. • Mean reflections, ○ first-order satellites, • second-order satellites.

of these components has been observed, we have not retained this six-dimensional hypothesis.

Now, we can also describe the structure with only one modulation vector, as in (1), but the general extinction rule $k + l = 2n$ is not verified by first-order satellites. We must conclude that the basic structure lattice is primitive; the four-dimensional Bravais class is $U^{Pmmm}_{1\,1\,1}$ with WJJ notations (de Wolff *et al.*, 1981). According to the recent WPV classification of the mono-incommensurate point groups (Weigel, Veysseyre & Phan, 1984; Veysseyre, Phan & Weigel, 1985; Veysseyre & Weigel, 1987), it belongs to the system orthogonal parallelogram rectangle (point group 2,*m*,*m*). Refinement of the structure at 100 K in this hypothesis has already been achieved (Sciau *et al.*, 1986) and results are in good agreement with the space group $U^{P2_1nb}_{1\,qq}$ or $F(2,3,4)\ 2_a, m_{a+(c+d)/4}, m_{(b+d)/4}$ in WPV notations.

In such a group, and according to the cell transformation $\mathbf{A} = \mathbf{a}$, $\mathbf{B} = 2\mathbf{b}$, $\mathbf{C} = 2\mathbf{c}$ which allows elimination of the rational components of the wavevector, the pattern has to obey the following extinction rules:

HKLm:	$K + m = 2n$	centring U or $F(2,3,4)$
	$L + m = 2n'$	
H0Lm:	$2H + L + m = 4n$	mirror plane (n) or $m_{a+(c+d)/4}$
HK0m:	$K + m = 4n$	mirror plane (b) or $m_{(b+d)/4}$
H00m:	$H = 2n$	axis (2_1) or 2_a.

Unfortunately, these are not verified by second-order satellites; for each, there are a few weak reflections which are significatively non-zero and transgress the rules. Moreover, from our measurements the systematic extinction of the following lines can be shown:

$$hkl0: \quad k + l = 2n + 1$$
$$hkl\pm2: \quad k + l = 2n + 1;$$

this is not explained in our last hypothesis.

We have now to consider a lower symmetry: the monoclinic one.

We suppose that the eight satellites around each Bragg node are the juxtaposition of two groups of four satellites: $\pm(\xi,\frac{1}{2},\frac{1}{2})$ and $\pm(\xi,-\frac{1}{2},-\frac{1}{2})$ for the first group, $\pm(\xi,-\frac{1}{2},\frac{1}{2})$ and $\pm(\xi,\frac{1}{2},-\frac{1}{2})$ for the second (Fig. 1). We could here suppose two independent modulation vectors (ii), but this would not explain the observed splitting of the main reflections along $\mathbf{b}^*$ (Saint-Grégoire *et al.*, 1986; Ryan, 1986), and so we retain only the hypothesis (iii). Each group corresponds to a twin domain and the crystal is composed of two twin domains of monoclinic symmetry, with the unique axis along $\mathbf{a}$ and with an angle very close to 90°. The mirror planes m_y and m_z are now pseudosymmetry operations and each domain is related to the other by these symmetry operations.

In such an hypothesis, all reflections can be indexed with a unique modulation vector and the pattern is compatible with an A-centred lattice (space group $A2_111$). The transformation

$$\mathbf{a}' = \mathbf{a},\ \mathbf{b}' = (\mathbf{b} + \mathbf{c})/2,\ \mathbf{c}' = (\mathbf{b} - \mathbf{c})/2$$

gives an equivalent primitive lattice (space group $P2_1$) and the modulation vector is $\mathbf{q}^* = \zeta\mathbf{a}'^* + \frac{1}{2}\mathbf{b}'^*$ ($\mathbf{a}'^*,\mathbf{b}'^*,\mathbf{c}'^*$: basic reciprocal vectors).

This can be written $\mathbf{q}^* = \mathbf{q}_i^* + \mathbf{q}_r^*$ with $\mathbf{q}_i^* = \zeta\mathbf{a}'^*$ and $\mathbf{q}_r^* = \frac{1}{2}\mathbf{b}'^*$. The four-dimensional Bravais class is $B^{P2/m}_{1\,1}$ (WJJ) or diorthogonal parallelograms $S(2,4)\ 2\perp2$ (WPV), and superspace group $B^{P2_1}_{1}$ (WJJ) or $S(2,4)2_a$ (WPV).

In order to maintain compatibility with the previous orthorhombic descriptions and with the HT cell, and to permit easy indexing in the pseudo-orthorhombic symmetry, we have chosen to keep the orthorhombic cell (**A**, **B**, **C**). The superspace group is now $U^{A2_111}_{1\,11}$ (WJJ) or $F(2,3,4)\ 2_a$ (WPV) and the extinction conditions for a domain are:

HKLM:	$K + M = 2n$	
	$L + M = 2n'$	centring (e_4, B), (e_4, C), (B, C)
	$(K + L = 2n'')$	
	$K + L + 2M = 4n$	A centring ($k + l = 2n$)
H00M:	$H = 2n$	axis (2_1) or 2_a.

These new conditions are now quite satisfactory to describe the diffraction pattern; they are verified by all the reflections and do not omit any other extinction of the pattern. Thus, they will be retained as the basis of the present structure refinement.

Structure refinement

The space group of the average structure in its monoclinic symmetry is $A2_111$, using the pseudo-orthorhombic setting of the axes.

The displacive modulation $\mathbf{u}^\mu$ of the μth atom can be defined by the atomic displacement coordinates u_i^μ from the average positions $\bar{x}_i^\mu$.

$$u_i^\mu = x_i^\mu - \bar{x}_i^\mu \quad (i = 1, 3) \qquad (3)$$

These displacements are periodic functions of the variable $\bar{x}_4^\mu = \mathbf{q}.\mathbf{x}^\mu + t$, where t is a phase variable. Following Yamamoto (1982*a*), these can be written by their Fourier series:

$$u_i^\mu(\bar{x}_4^\mu) = \{A_{ni}^\mu \cos(2\pi n\bar{x}_4^\mu) + B_{ni}^\mu \sin(2\pi n x_4^\mu)\}, \qquad (4)$$

where n is the order of the Fourier term, and A_{ni}^μ and B_{ni}^μ are the Fourier amplitudes.

There are six independent atoms in general positions and, consequently, 18 independent positional parameters for the average structure ($\bar{x}_i^\mu$), and 36 independent parameters of the Fourier amplitudes for each order of harmonics of modulation in the preceding development (4), (A_{ni}^μ, B_{ni}^μ). As temperature B factors have not been modulated, there are respectively 6 and 36 independent parameters for the isotropic and anisotropic temperature factors.

The least-squares program *REMOS* (Yamamoto, 1982*b*) has been used for the refinement. It calculates

Table 1. *R_F factors (%) for the monoclinic hypothesis (100 K and 210 K) and for the orthorhombic hypothesis (210 K)*

Space group	$U^{A2_1 11}_{1\,11}$		$U^{A2_1 11}_{1\,11}$		$U^{P2_1 nb}_{1\,qq}$	
Temperature	100 K		210 K		210 K	
Fourier terms	1,2*		1,2*		1,2*	
R_F $m=0$	3·0	[657]†	3·2	[669]	3·8	[404]
R_F $m=\pm1$	4·9	[2567]	7·2	[2476]	8·1	[1316]
R_F $m=\pm2$	8·2	[1097]	16·7	[699]	41·7	[497]
R_F All	4·51	[4321]	5·61	[3844]	8·1	[2217]
Independent parameters	126		126		125	

* The anisotropic temperature factors have been refined for reflections with $0{\cdot}38 \le (\sin\theta)/\lambda \le 0{\cdot}71$ Å^{-1} (3572 at 100 K and 3183 at 210 K).

† The numbers of reflections are given in square brackets. Reflections *HKLM* and *HK̄LM* are equivalent in the orthorhombic hypothesis.

the structure factors using the preceding four-dimensional analysis and minimizes the reliability factor *wR*:

$$wR = \sum_i w_i(|F_{oi}| - |F_{ci}|)^2/\sum_i w_i|F_{oi}|^2, \qquad (5)$$

in which w_i is a weight factor, and F_{oi} and F_{ci} are the observed and calculated structure factors. Unit weights have been used for all reflections. The atomic scattering factors have been taken from *International Tables for X-ray Crystallography* (1974).

The program can take into account twinning of the crystal. The relative ratio between the twin volumes is a new refinement parameter. In the present study, we have considered incoherent twin domains, *i.e.* the observed intensity of a diffraction line is the summation of the intensities relative to each domain. But it was practically impossible to take into account simultaneously this twinning and a secondary-extinction correction.

Refinement of temperature factors was very sensitive and difficult because of strong correlations with each other and with modulation parameters. This is why it would be meaningless to try to modulate them. When refined with all the observed reflections [$(\sin\theta)/\lambda < 0{\cdot}71$ Å^{-1}], they became physically non-significant. This can be explained by the influence of intense peaks with lower values of θ, for which no secondary-extinction correction could be calculated. After several trials, we have obtained reasonable values when eliminating reflections with $(\sin\theta)/\lambda < 0{\cdot}38$ Å^{-1}. They were then constrained to these values for the final refinement.

Another difficulty has been outlined and concerns correction of temperature Debye–Waller factors for phase fluctuations (Axe, 1980; Adlhart, 1982; Paciorek & Kucharczyk, 1985). It has been shown that the presence of phase propagation waves involves a lowering of the intensity of the higher-order satellites. Effectively, our results have shown that the calculated values of the intensities of the second-order satellites are generally higher than the observed ones. We have tried a phason correction but this did not improve our results. This systematic misfit on second-order satellites seems to be correlated more with refinement difficulties and with the fact that we did not take into account modulation harmonics and satellites of higher order. Satellites up to the third order have been observed, which would tend to prove that a phason correction should in any case be weak.

Table 2. *Final parameters at 100 and 210 K in the space group $A^{2_1 11}_{1\,11}$ (cell A, B, C)*

(*a*) Positional parameters (×10⁴)

		Average position	A_1	B_1	A_2	B_2
At 100 K						
Ba	x_1	4480*	128†	211 (1)	−23 (1)	46 (2)
	x_2	1724·6 (1)	38·3 (3)	49·5 (3)	2·7 (4)	25·3 (2)
	x_3	2503 (1)	−9 (1)	−4 (1)	13 (2)	−9 (2)
Mn	x_1	−51 (2)	−21 (3)	−17 (3)	−4 (3)	26 (3)
	x_2	2080·8 (3)	3·5 (5)	−5·3 (5)	17·3 (5)	2 (5)
	x_3	42 (3)	40 (2)	17 (2)	2 (5)	−11 (4)
F(1)	x_1	1962 (7)	7 (10)	−31 (11)	−7 (12)	49 (12)
	x_2	1497 (2)	11 (2)	−7 (2)	16 (2)	5 (2)
	x_3	31 (10)	95 (8)	205 (7)	36 (14)	−33 (16)
F(2)	x_1	7195 (7)	−89 (11)	26 (10)	−28 (11)	43 (12)
	x_2	1685 (2)	43 (2)	−10 (2)	20 (2)	4 (3)
	x_3	−16 (9)	−62 (8)	−139 (8)	−18 (15)	3 (15)
F(3)	x_1	3346 (7)	−87 (11)	−18 (10)	−37 (12)	21 (12)
	x_2	2320 (2)	13 (3)	−5 (2)	21 (2)	7 (2)
	x_3	−27 (11)	−269 (8)	−124 (8)	−25 (18)	44 (18)
F(4)	x_1	214 (8)	322 (12)	114 (12)	−46 (14)	43 (16)
	x_2	2111 (2)	43 (3)	106 (2)	20 (3)	−8 (3)
	x_3	2487 (9)	26 (9)	8 (9)	−3 (15)	−2 (14)
At 210 K						
Ba	x_1	4480*	128†	141 (2)	−2 (2)	38 (3)
	x_2	1722·7 (2)	35·6 (4)	30·5 (4)	4·6 (4)	12·7 (3)
	x_3	2504 (2)	−9 (1)	−2 (1)	6 (2)	−11 (2)
Mn	x_1	−50 (2)	−14 (3)	−10 (3)	3 (5)	7 (5)
	x_2	2080·6 (3)	1·6 (6)	−4·9 (5)	6·6 (7)	−1·5 (7)
	x_3	15 (5)	32 (2)	5 (2)	13 (6)	−22 (5)
F(1)	x_1	1976 (7)	1 (10)	−19 (11)	7 (18)	−3 (18)
	x_2	1500 (2)	6 (2)	−6 (2)	4 (3)	−3 (3)
	x_3	73 (10)	97 (9)	129 (8)	15 (17)	−52 (17)
F(2)	x_1	7213 (8)	−61 (13)	13 (12)	−10 (18)	28 (18)
	x_2	1680 (2)	27 (3)	−11 (3)	11 (3)	−1 (3)
	x_3	−56 (10)	−68 (9)	−96 (9)	−22 (17)	21 (16)
F(3)	x_1	3347 (8)	−56 (13)	13 (12)	−4 (20)	−15 (22)
	x_2	2319 (2)	7 (3)	−12 (3)	10 (3)	3 (3)
	x_3	−34 (12)	−237 (10)	−71 (10)	15 (22)	73 (18)
F(4)	x_1	245 (10)	248 (15)	60 (16)	−83 (24)	15 (30)
	x_2	2110 (2)	48 (4)	79 (3)	6 (4)	−13 (5)
	x_3	2518 (13)	18 (12)	9 (10)	−41 (20)	−46 (20)

(*b*) Equivalent isotropic temperature factors (Å²)

	100 K	210 K		100 K	210 K
Ba	0·46 (1)	0·79 (2)	F(2)	0·73 (7)	0·93 (9)
Mn	0·34 (2)	0·51 (2)	F(3)	0·74 (7)	1·17 (9)
F(1)	0·55 (7)	0·68 (8)	F(4)	1·14 (8)	2·1 (1)

* Fixed to define the cell origin along the polar axis.
† Fixed to define the phase origin.

Results

The *R* factors at 100 and 210 K (space group $U^{A2_1 11}_{1\,11}$) are given in Table 1 and final refinement parameters are in Table 2. For comparison, *R* factors at 210 K for

orthorhombic symmetry (space group $U^{P2_1nb}_{1\,qq}$) are also given in Table 1.*

For an equivalent number of independent refinement parameters, the R factors are better in the monoclinic description. This is particularly true for the R factor calculated with only second-order satellites ($m = \pm 2$). These results clearly confirm our choice of monoclinic symmetry.

It can be noted here that the R factors for $m = \pm 2$ are rather large, and still larger at 210 K for 699 reflections than at 100 K for 1097 reflections. This has to be related to an experimental fact: intensities of these satellite reflections are much weaker than those of the first-order satellites at the same temperature, or weaker at 210 K than at 100 K. Consequently, for the same absolute average discrepancy between observed and calculated structure factors, the reliability factor will be higher.

It is interesting now to compare the results obtained at both temperatures: R factors are better at 100 K than at 210 K and this with a higher number of satellite reflections. They are measured better, not only because of the weakening of thermal vibration, but also because of their higher intensity, related to the evolution of the modulation. This is in agreement with the classical model of evolution of the modulated structures, which predicts an increase of the amplitude of modulation when cooling the sample.

We have tried to check another general property predicted by the theory: the shape of the modulation wave is smooth and purely harmonic just below the HT transition and splits and progressively shows gaps when cooling. The modulation function becomes near a Heaviside function and its Fourier series should present only odd terms. Thus we have tried to introduce third-order Fourier terms into our refinement. Third-order measured satellites were too few or too weak to be significant in the calculation, but it can be shown that an important amplitude of the third-order Fourier terms will influence the other intensities and particularly those of the second-order satellites. Results are summarized in Tables 3 and 4. Unexpectedly, there was no significant improvement and, in any case, second-order Fourier terms are always necessary for good agreement. Odd-order Fourier terms only are not sufficient to describe the modulation and, when keeping second-order satellites, there is no significant change of the refinement parameters as can be seen in Table 4. For the displacement of Ba, for example, Fourier terms A_3 and B_3 remain very weak. In contrast, we only observe important second-order terms in relation to important first-order terms and the ratio between these respective terms remains about the same at both temperatures. Consequently, we could not conclude that there was significant evolution of the modulation function shape to the Heaviside function from 210 to 100 K. This function appears to be a pure harmonic function corrected by asymmetrical second-order harmonics. This result is not incompatible with the presence of discontinuities of the modulation function or with the presence of discommensurations in the crystal, but outlines an asymmetry of the amplitude of modulation in the range of the microdomains between two eventual discommensurations. From our present results, we cannot draw any further conclusion concerning the characterization of these discommensurations or the presence of crystal faults in relation to these discommensurations or with the low-temperature variation of ξ.

Table 3. *R_F factors (%) as a function of the order of refined Fourier terms*

		210 K		100 K	
Fourier terms		1,3	1,2,3	1,3	1,2,3
R_F	$m = 0$	3·7	3·1	5·8	3·0
	$m = \pm 1$	10·3	7·1	12·7	4·8
	$m = \pm 2$	29·5	16·3	36·9	7·4
	All	8·1	5·5	12·6	4·4
Independent parameters		126	162	126	162

Table 4. Ba *positional parameters* ($\times 10^4$) *along the direction of important displacement*

(1) Refinement to the second-order Fourier term.
(2) Refinement to the third-order Fourier term.

	Average position	A_1	B_1	A_2	B_2	A_3	B_3
At 210 K							
$x_1^{(1)}$	4480*	128†	141 (2)	−2 (2)	38 (3)		
$x_1^{(2)}$	4480*	128†	141 (2)	0 (2)	42 (3)	21 (5)	−17 (6)
x_2	1722·7 (2)	35·6 (4)	30·5 (4)	4·6 (4)	12·7 (3)		
x_2	1722·6 (2)	35·6 (3)	30·5 (4)	5·2 (4)	13·1 (3)	2 (1)	0 (2)
At 100 K							
x_1	4480*	128†	211 (1)	−23 (1)	46 (2)		
x_1	4480*	128†	211 (1)	−23 (1)	46 (2)	19 (3)	1 (3)
x_2	1724·5 (1)	38·3 (3)	49·5 (3)	2·7 (4)	25·3 (2)		
x_2	1724·5 (1)	38·3 (3)	49·4 (3)	3·3 (4)	25·4 (2)	0 (1)	1 (1)

* Fixed to define the cell origin along the polar axis.
† Fixed to define the phase origin.

Discussion

One of the refinement parameters is the relative ratio of the volumes of the two monoclinic twin domains of the crystal. It has been refined to 42% at 210 K and to 52% at 100 K. These proportions are nearly equivalent to the ratio of 50% and are thus compatible with the apparent orthorhombic symmetry of the pattern, as far as reflections from each domain are almost equivalent in intensity and indistinguishable in position. The tiny discrepancy between the two

* Lists of structure factors and anisotropic thermal parameters have been deposited with the British Library Document Supply Centre as Supplementary Publication No. SUP 44477 (86 pp.). Copies may be obtained through The Executive Secretary, International Union of Crystallography, 5 Abbey Square, Chester CH1 2HU, England.

refinements can be explained by thermal history: the sample has been brought again to room temperature in the HT phase between both data collections, and so it has recovered its fundamental orthorhombic symmetry. After this relaxation, and when cooling again below 250 K, the sample is likely to divide itself into two twin domains with another twin ratio. It would be interesting to study here the influence of an oriented strain distribution applied to the crystal during its orthorhombic–monoclinic phase transition on the related intensities of each twin domain.

The two types of domains are related to each other by a mirror plane, m_y. If we neglect the elastic strain of the cell ($\alpha \sim 90{\cdot}08°$), their relative structures differ only by the orientations of their wavevectors $\mathbf{q}^*$. This structure is drawn schematically for one domain in Figs. 2, 3 and 4. The atomic displacements are very similar at 100 and 210 K, as can be seen for example for the Ba displacements along x_1 and x_2 in Fig. 2. When considered together, they are consistent with a rigid-body rotation of the MnF_6 octahedra, around an axis parallel to their edges, F(1)–F(2), F(3)–F(3)^i. This movement is coupled with a motion of the Ba ions in the plane (x_1, x_2), following the motion of the nearest F(4) ion (Fig. 3). As can be seen in Fig. 3, the x_1 and x_2 displacements have the same phase and we can conclude that there is a linear movement of the Ba ions. One can also point out the similarity of the two curves at 100 and 210 K, obtained with two independent measurements and refinements.

Interatomic distances are listed in Table 5 and drawn schematically in Fig. 5 for Ba–F species, as a function of the phase variable t. Their average values are compatible with those of the HT phase. Let us first consider the distances Mn–F and F–F which characterize the deformation of the MnF_6 octahedra: their variations in the modulated structure are weak (respectively 2 and 5% for Mn–F and F–F distances). They are clearly smaller than the absolute displacements of the corresponding atoms and remain in the range of their standard deviations; this clearly confirms the hypothesis of a rigid-body motion of the octahedra. These conclusions are still true for the refinement at 100 K, for which the amplitudes of the modulation functions are larger, and standard deviations are smaller; *i.e.* the variations of the interatomic distances seem to be related to the accuracy of the refined positional parameters. Nevertheless, one can notice a weak deformation of the octahedra due to the motion of the F(2) atom. If we consider now the Ba–F distances (Fig. 5), we clearly see that there is no significant variation of the shorter distances [Ba–F(1), Ba–F(1)^{iii}, Ba–F(4), Ba–F(3)]; *i.e.* the neighbouring atoms move

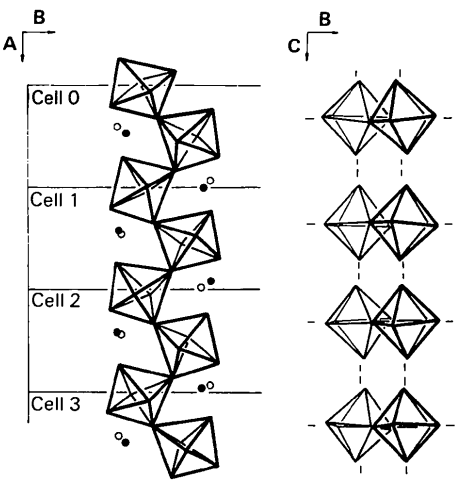

Fig. 3. Schematic representation of the projection of a slab of octahedra along the A direction over four cells (displacement ×1·5): • Ba, $x_3 = \frac{1}{4}$; ○ Ba, $x_3 = -\frac{1}{4}$.

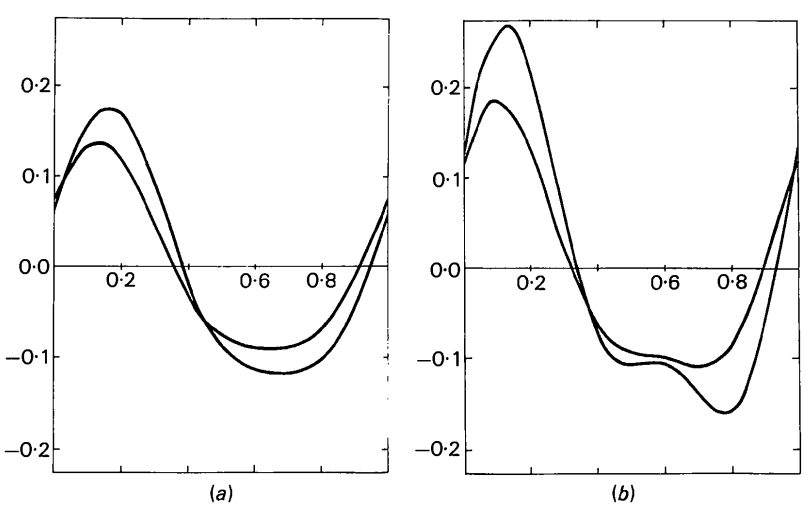

Fig. 2. Ba displacements (Å) (*a*) along x_1 and (*b*) along x_2 as a function of x_4'' at 100 and 210 K.

in phase. On the other hand, the larger distances [Ba–F(4)^{iv}, Ba–F(2)^{iv} and Ba–F(3)^{v}] present variations which are about twice the corresponding atomic displacements, and which can be explained by relative motions in opposition of phase.

The rotation of the MnF_6 octahedra which is involved is compatible with a compacting of the HT structure along the x_1 and x_2 directions, which is in good agreement with the evolution of the cell parameters as a function of temperature (Cox *et al.*, 1979).

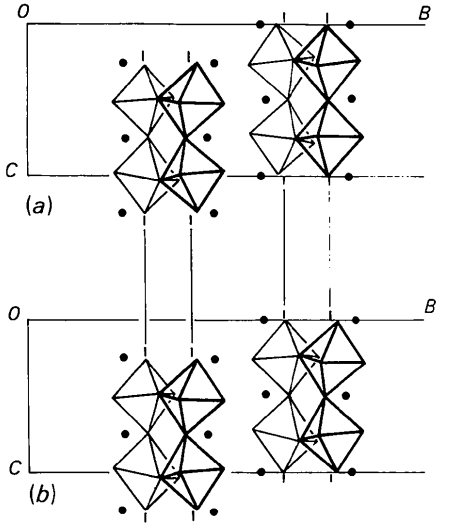

Fig. 4. Schematic representation of the projection along the **A** direction of two neighbouring slabs (*a*) in space group $U^{P2_1^{nb}}_{1qq}$ and (*b*) in space group $U^{A2_111}_{1\,11}$.

Conclusion

An important result of the present study of the structure of $BaMnF_4$ is the very good agreement of the harmonic model of modulation with the atomic displacement functions. Harmonics up to second order are necessary and adequate to obtain a very satisfactory agreement. The physical significance of these terms is proved:

– from a comparison of and the analogy between the results of independent measurements and refinements at 210 and 100 K.

– from a consideration of the interatomic distances which are constant within the range of their standard deviations, for neighbouring species, both at 100 K and at 210 K, and which are comparable to those of the HT phase. The constancy of these interatomic distances as a function of the phase of the modulation shows that the atomic displacements are compatible with a rigid-body motion of the MnF_6 octahedra. This motion can be approximated by a rotation around the A axis.

The only significant difference between both modulated structures at 100 and 210 K concerns the amplitude of the displacements, which increase at low temperature. As far as the shape of the modulation wave is concerned, we could not show any significant evolution. The relative influence of first- or second-order terms in the Fourier series is the same, and introduction of higher-order terms did not really improve the reliability, as we could expect for a less harmonic function. An initial explanation could be that we have not enough high-order satellites to refine higher-order terms of the Fourier series and, to confirm our results, it would be good to have another data

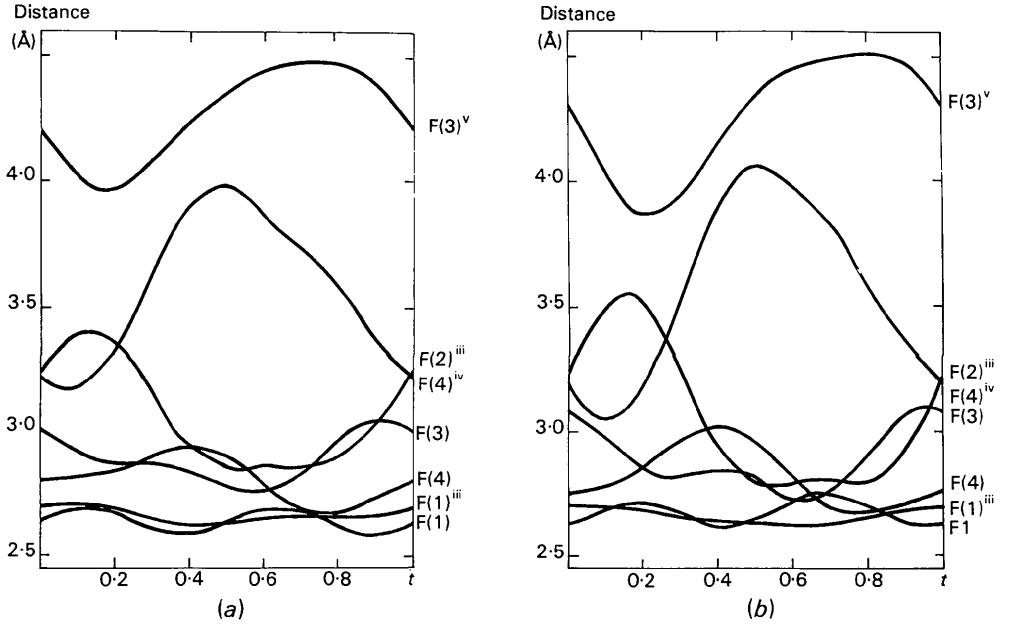

Fig. 5. Ba–F interatomic distances as a function of the phase variable at (*a*) 210 K and (*b*) 100 K ($t = \bar{x}_4^{\mu} - \xi\bar{x}_1^{\mu}$).

Table 5. *Interatomic distances* (Å) *at* 100 *and* 210 K

	Average	Maximal	Minimal	Variation
At 100 K				
Mn–F(1)	2·15 (5)	2·15	2·13	0·02
Mn–F(2)	2·00 (5)	2·05	1·94	0·11
Mn–F(3)	2·18 (8)	2·20	2·15	0·05
Mn–F(3)^{i}	2·06 (8)	2·09	2·05	0·04
Mn–F(4)	2·09 (7)	2·13	2·07	0·06
Mn–F(4)^{ii}	2·18 (7)	2·22	2·14	0·08
F(1)–F(2)	2·87 (14)	2·96	2·79	0·18
F(1)–F(3)	2·64 (13)	2·67	2·61	0·06
F(1)–F(4)	2·99 (17)	3·08	2·90	0·18
F(1)–F(4)^{ii}	3·04 (17)	3·14	2·97	0·17
F(2)–F(3)^{i}	3·09 (19)	3·21	2·96	0·25
F(2)–F(4)	3·04 (19)	3·22	2·88	0·34
F(2)–F(4)^{ii}	3·05 (19)	3·24	2·93	0·31
F(3)–F(3)^{i}	3·20 (18)	3·30	3·13	0·17
F(3)–F(4)	2·93 (18)	2·97	2·86	0·11
F(3)–F(4)^{ii}	2·97 (18)	3·08	2·85	0·23
F(3)^{i}–F(4)	2·94 (18)	2·98	2·91	0·07
F(3)^{i}–F(4)^{ii}	2·99 (18)	3·07	2·87	0·20
Ba–F(1)	2·68 (7)	2·74	2·63	0·11
Ba–F(1)^{iii}	2·65 (7)	2·70	2·62	0·08
Ba–F(2)^{iii}	3·05 (8)	3·52	2·79	0·73
Ba–F(3)	2·88 (7)	3·09	2·73	0·36
Ba–F(3)^{v}	4·26 (10)	4·52	3·87	0·65
Ba–F(4)	2·82 (6)	3·02	2·67	0·35
Ba–F(4)^{iv}	3·56 (8)	4·06	3·05	1·01
At 210 K				
Mn–F(1)	2·14 (6)	2·16	2·13	0·03
Mn–F(2)	2·05 (6)	2·09	2·01	0·08
Mn–F(3)	2·17 (9)	2·20	2·16	0·04
Mn–F(3)^{i}	2·07 (9)	2·08	2·04	0·04
Mn–F(4)	2·13 (10)	2·20	2·08	0·12
Mn–F(4)^{ii}	2·13 (10)	2·20	2·07	0·13
F(1)–F(2)	2·93 (15)	2·99	2·87	0·12
F(1)–F(3)	2·63 (14)	2·67	2·60	0·07
F(1)–F(4)	2·97 (18)	3·06	2·91	0·15
F(1)–F(4)^{ii}	3·04 (18)	3·11	2·94	0·17
F(2)–F(3)^{i}	3·12 (21)	3·22	3·00	0·20
F(2)–F(4)	3·13 (21)	3·27	2·93	0·34
F(2)–F(4)^{ii}	3·05 (18)	3·20	2·94	0·40
F(3)–F(3)^{i}	3·21 (20)	3·25	3·14	0·11
F(3)–F(4)	2·93 (20)	3·03	2·86	0·17
F(3)–F(4)^{ii}	2·98 (20)	3·11	2·85	0·26
F(3)^{i}–F(4)	2·96 (20)	3·07	2·88	0·19
F(3)^{i}–F(4)^{ii}	2·98 (20)	3·10	2·86	0·24
Ba–F(1)	2·64 (8)	2·69	2·56	0·11
Ba–F(1)^{iii}	2·66 (8)	2·72	2·62	0·10
Ba–F(2)^{iii}	3·06 (8)	2·86	3·40	0·54
Ba–F(3)	2·89 (9)	3·05	2·76	0·29
Ba–F(3)^{v}	4·27 (10)	4·48	3·98	0·50
Ba–F(4)	2·81 (9)	2·94	2·66	0·28
Ba–F(4)^{iv}	3·57 (11)	3·98	3·18	0·80

Symmetry codes: (i) $x_1-\frac{1}{2}$, $\frac{1}{2}-x_2$, $-x_3$, $x_4+\frac{1}{2}$; (ii) x_1, x_2, $\frac{1}{2}-x_3$, $x_4-\frac{1}{2}$; (iii) $x_1-\frac{1}{2}$, $\frac{1}{4}-x_2$, $\frac{1}{4}-x_3$, x_4; (iv) $x_1+\frac{1}{2}$, $\frac{1}{2}-x_2$, $\frac{1}{2}-x_3$, x_4; (v) $x_1+\frac{1}{2}$, $\frac{1}{2}-x_2$, $\frac{1}{2}-x_3$, $x_4+\frac{1}{2}$.

collection with a more intense source, in order to measure third- or even fourth-order satellites. Nevertheless, as has been explained above, second-order terms are refined with real accuracy and significance, and they seem to prove a real asymmetry of the modulation wave. This asymmetry is correlated with asymmetrical displacements in the structure on both sides of the average positions.

The analogy of the shapes of the modulation functions at 100 and 210 K can be correlated with the abnormal behaviour of $BaMnF_4$ with regard to the theoretical model of a progressive locking of the modulation to a commensurate superstructure coupled with a 'squaring' of the modulation function. In our case, no lock-in transition has been observed and the variation of the **q*** vector is very weak over a large temperature range. Thus, there is no reason here to expect any evolution towards a locked phase.

We have clearly confirmed in the present study the monoclinic hypothesis of the structure which explains very well the X-ray diffraction pattern symmetry. Nevertheless a comparison can be made with the orthorhombic description. The two descriptions have the same atomic refinement parameters and after refinement (with the measurements of 210 K), their values are quite similar. The two space groups ($U^{A2_1 11}_{1\ 11}$ and $U^{P2_1 nb}_{1\ qq}$) have half their symmetry operations in common and these operations generate all the atoms of one layer from the independent atoms. The others describe the passage of this layer to the nearest one. In the monoclinic description, this transformation is given by a pure translation $(I/0,\frac{1}{4},\frac{1}{4},0)$, and in the orthorhombic one by a glide mirror $(m_z/0,\frac{1}{4},\frac{1}{4},\frac{1}{4})$ which couples a mirror operation to a dephasing of the modulation. So, in the first case, all the octahedra layers are rigorously equivalent, which is not true in the second. Nevertheless, when we take into account the specific atomic positions of this structure, the new atomic positions generated by the glide mirror are nearly the translated positions, as can be seen in Fig. 4, and this explains the rather good agreement obtained in the first study. We have now concluded that two types of macrodomains related by an m_y mirror are present and we have given their relative volume ratio which is likely to depend on the phase-transition conditions.

References

ADLHART, W. (1982). *Acta Cryst.* A**38**, 498–504.

AXE, J. D. (1980). *Phys. Rev. B*, **21**(10), 4181–4190.

BARTHÈS-RÉGIS, M., ALMAIRAC, R., SAINT-GRÉGOIRE, P., FILIPPINI, C., STEIGENBERGER, U., NOUET, J. & GESLAND, J. Y. (1983). *J. Phys. Lett.* **44**, 829–835.

COX, D. E., SHAPIRO, S. M., COWLEY, R. A., EIBSCHÜTZ, M. & GUGGENHEIM, H. J. (1979). *Phys. Rev. B*, **19**, 5754–5772.

COX, D. E., SHAPIRO, S. M., NELMES, R. J., RYAN, T. W., BLEIF, H. J., COWLEY, R. A., EIBSCHÜTZ, M. & GUGGENHEIM, H. J. (1983). *Phys. Rev. B***28**, 1640–1643.

DVORAK, V. (1975). *Phys. Status Solidi B*, **71**, 269–275.

DVORAK, V. & FOUSEK, J. (1980). *Phys. Status Solidi A*, **61**, 99–105.

ESCANDE, A. (1971). Thesis, USTL Montpellier, France.

International Tables for X-ray Crystallography (1974). Vol. IV. Birmingham: Kynoch Press. (Present distributor D. Reidel, Dordrecht.)

KEVE, E. T., ABRAHAMS, S. C. & BERNSTEIN, J. L. (1969). *J. Chem. Phys.* **51**, 4928–4936.

PACIOREK, W. A. & KUCHARCZYK, D. (1985). *Acta Cryst.* A**41**, 462–466.

RYAN, T. W. (1986). *J. Phys. C*, **19**, 1097–1106.

SAINT-GRÉGOIRE, P. (1985). Thesis, USTL Montpellier, France.

SAINT-GRÉGOIRE, P., ALMAIRAC, R., FREUND, A. & GESLAND, J. Y. (1986). *Ferroelectrics*, **67**, 15–21.

SCIAU, PH., GREBILLE, D., BÉRAR, J. F. & LAPASSET, J. (1986). *Mater. Res. Bull.* **21**, 843–851.

VEYSSEYRE, R., PHAN, T. & WEIGEL, D. (1985). *C. R. Acad. Sci.* **300**, 51–54.

VEYSSEYRE, R. & WEIGEL, D. (1987). *Acta Cryst.* A**43**, 294–304.

WEIGEL, D., VEYSSEYRE, R. & PHAN, T. (1984). *C. R. Acad. Sci.* **298**, 825–828.
WOLFF, P. M. DE, JANSSEN, T. & JANNER, A. (1981). *Acta Cryst.* A**37**, 625–636.
YAMAMOTO, A. (1982*a*). *Acta Cryst.* A**38**, 87–92.
YAMAMOTO, A. (1982*b*). *REMOS*. A computer program for the refinement of modulated structures. National Institute for Research in Inorganic Materials, Niihari-gun, Ibaraki, Japan.

Acta Cryst. (1988). B**44**, 116–120

Structures of the ZrO_2 Polymorphs at Room Temperature by High-Resolution Neutron Powder Diffraction

BY C. J. HOWARD

Australian Nuclear Science and Technology Organisation, Lucas Heights Research Laboratories, Private Mail Bag 1, *Menai, New South Wales* 2234, *Australia*

R. J. HILL

CSIRO Division of Mineral Chemistry, PO Box 124, *Port Melbourne, Victoria* 3207, *Australia*

AND B. E. REICHERT

Research Group, ICI Australia Operations Pty Ltd, Newsom Street, Ascot Vale, Victoria 3032, *Australia*

(*Received* 7 *July* 1987; *accepted* 14 *October* 1987)

Abstract

The crystal structures of monoclinic ZrO_2 [$P2_1/c$, $a = 5{\cdot}1505\ (1)$, $b = 5{\cdot}2116\ (1)$, $c = 5{\cdot}3173\ (1)$ Å, $\beta = 99{\cdot}230\ (1)°$, $V = 140{\cdot}88\ (1)$ Å^3, $Z = 4$, $R_{wp} = 0{\cdot}047$], tetragonal $Zr_{0{\cdot}935}Y_{0{\cdot}065}O_{1{\cdot}968}$ [$P4_2/nmc$, $a = 3{\cdot}6055\ (1)$, $c = 5{\cdot}1797\ (2)$ Å, $V = 67{\cdot}33\ (1)$ Å^3, $Z = 2$, $R_{wp} = 0{\cdot}090$] and cubic $Zr_{0{\cdot}875}Mg_{0{\cdot}125}O_{1{\cdot}875}$ [$Fm3m$, $a = 5{\cdot}0858\ (1)$ Å, $V = 131{\cdot}55\ (1)$ Å^3, $Z = 4$, $R_{wp} = 0{\cdot}083$] have been refined by Rietveld analysis of 1·377 Å neutron powder diffraction data collected at 295 K. In both tetragonal and cubic ZrO_2, the stabilizer atoms randomly occupy the Zr site and charge balance is achieved by an appropriate number of vacancies on the O site. In cubic ZrO_2, the anions are displaced from their ideal fluorite positions by $0{\cdot}025a$ in the [111] direction and there is evidence for the presence of either a small quantity of a tetragonal impurity phase, or a slight tetragonal distortion.

Introduction

Pure zirconia, ZrO_2, is monoclinic at room temperature, tetragonal between ~1440 and ~2640 K, and cubic up to the melting point at ~2950 K. The monoclinic phase is a distortion of the fluorite (CaF_2) structure with the Zr atom in seven coordination. In both high-temperature phases, the Zr atom assumes eight coordination, as in fluorite, but in the tetragonal form the O atom is substantially displaced from its ideal fluorite $\frac{1}{4},\frac{1}{4},\frac{1}{4}$ position. The tetragonal and cubic phases of pure zirconia can be stabilized at room temperature by the addition of suitable oxides, namely MgO, CaO, Sc_2O_3, Y_2O_3 and certain rare-earth oxides. An orthorhombic form has also been prepared by quenching from high pressure and temperature (Suyama, Ashida & Kume, 1985) but this phase will not be considered further here.

The crystal structures of, and mechanisms of the transformations between, the monoclinic, tetragonal and cubic phases are of considerable technical interest since they can be manipulated to provide optimized physical and chemical properties of the materials fabricated from the stabilized zirconia (Garvie, Hannink & Pascoe, 1975; Roth, 1975; Claussen, Ruhle & Heuer, 1984; Fisher, 1986). The so-called partially stabilized zirconias (PSZ), which are typically two-phase cubic and tetragonal or single-phase tetragonal, are of importance for mechanical and structural applications. The fully stabilized zirconias (FSZ), which are normally single-phase cubic, are of interest for heating elements, oxygen sensors and fuel-cell applications.

Crystal structure determinations have been performed on tetragonal ZrO_2 using X-ray powder diffraction intensities collected at 1470 to 2230 K by Teufer (1962). Monoclinic ZrO_2 (baddeleyite) has been studied at room temperature using X-ray single-crystal methods by McCullough & Trueblood (1959) and Smith & Newkirk (1965). Cubic $Zr(Ca,Y)O_{2-x}$ solid solutions have been analyzed at various temperatures from both X-ray and neutron data by Carter & Roth (1968), Steele & Fender (1974), Faber, Mueller & Cooper (1978), Morinaga, Cohen & Faber (1979) and Horiuchi, Schultz, Leung & Williams (1984).

0108-7681/88/020116-05$03.00